INTERNATIONAL JOURNAL OF AGRICULTURE & BIOLOGY
ISSN Print: 1560–8530; ISSN Online: 1814–9596
24–0518/2025/33330406
DOI: 10.17957/IJAB/15.2296
http://www.fspublishers.org

Full Length Article

Reflectance Versus Fluorescence Imaging: ANN-Based Approach for Predicting Phenol Content on Red Betel Leaves

Retno Damayanti[1,2*], Yusuf Hendrawan[2†], Sandra[2†] and Bambang Dwi Argo[2†]
[1]*Department of Agroindustrial Technology, Universitas Brawijaya, Malang 65145, Indonesia*
[2]*Department of Biosystems Engineering, Universitas Brawijaya, Malang 65145, Indonesia*
[*]For correspondence: damayanti@ub.ac.id
[†]Contributed equally to this work and are co-first author
Received 17 October 2024; Accepted 12 December 2024; Published online 25 December 2024

Editor: Abdul Wahid

Abstract

Identification systems using computer vision are important in image recognition technology and artificial intelligence in the agricultural sector. Identifying the phenol content in red betel leaves (*Piper crocatum* Ruiz & Pav.) using computer vision made it possible to predict the phenol content quickly and efficiently, simplifying the process of classifying product quality. This research used computer vision methods combined with artificial neural networks (ANN) using reflectance and fluorescence images to obtain predictive modeling of phenol content in red betel leaves. The research was aimed to compare the ANN model to predict the phenol content in red betel leaves using reflectance and fluorescence images. The ANN model used 75 data from reflectance images, 75 data from fluorescence images, and 75 data from total phenol content. The color features of the image were used as input data and the total phenol content was used as output data. The dataset used was 75% as cumulative data and 25% as validation data. From the reflectance data, the best architecture chosen was 20-30-1 with a learning rate of 0.1, a momentum of 0.9, tansig as the activation function in the hidden layers, purelin as the activation function in the output layer, and trainlm as the learning function, which produced an MSE value of 0.0090, validation MSE of 0.0880, training R of 0.9777, and validation R 0.7944. Meanwhile, from the fluorescence data, the best architecture chosen was 20-10-1 with a learning rate of 0.1, momentum 0.9, tansig as activation function in the hidden layers, purelin as activation function in the output layer, and trainlm as a learning function, which produced an MSE value of 0.0099, validation MSE of 0.4368, training R of 0.9796, validation R of 0.4436. The reflectance imaging produced the best ANN modeling for predicting the phenol content of red betel leaves.

Keywords: Fluorescence; Phenol; Red Betel; Reflectance

Introduction

Red betel leaf (*Piper crocatum* Ruiz & Pav.) is one of the herbal plants that has many health benefits, especially because of its high phenol content. Phenol is a bioactive compound with antioxidant activity that is important for protecting the body from free radicals. Phenol is a secondary metabolite that is the source of all benzene groups produced by plants (Edo *et al.* 2024). Red betel leaf has several pharmacological activities including as an antioxidant, antibacterial, anti-inflammatory, and antiseptic (Singh *et al.* 2023; Tran *et al.* 2023). Therefore, it is important to develop an effective method to measure and predict phenol levels in red betel leaves to ensure their quality and benefits.

Image-based sensing technology has been widely used in agriculture and food science to analyze bioactive compounds in plants non-destructively. Two popular methods in analyzing plant compounds are reflectance imaging and fluorescence imaging, which can provide important information about the optical properties and chemical composition of plants. Both methods allow for fast and efficient measurements without damaging the sample, making them a more practical alternative to conventional chemical methods. Non-destructive measurements utilize computer vision, which works based on an image to make useful decisions about real physical objects (Chan 2010). Computer vision allows computers to interpret and understand the visual world in a way that is similar to human vision. Identification systems using computer vision

To cite this paper: Damayanti R, Y Hendrawan, Sandra, BD Argo (2025). Reflectance versus fluorescence imaging: ANN-based approach for predicting phenol content on red betel leaves. *Intl J Agric Biol* 33:330406. https://doi.org/10.17957/IJAB/15.2296

have an important role in image recognition technology and artificial intelligence in agriculture. With the ability to process and analyze images automatically, computer vision can improve the efficiency of decision making in agriculture, such as computer vision for detection of food nutrients (Kaushal *et al*. 2024), non-destructive evaluation of agricultural products (Li *et al*. 2024), identification for quality and safety of small berry fruits (Li *et al*. 2019).

The appearance of materials related to color, shape, and surface texture, is often used as a visual inspection in product evaluation or sorting. Visual inspection carried out by human operators is still limited in terms of speed, volume, and subjectivity. Therefore, that computer vision applications have been developed where the human eye is replaced by a camera and the brain is replaced by a computer (Lu *et al*. 2020). One of the applications of computer vision in agriculture is measuring the content in objects based on the results of reflectance and fluorescence-based image processing. Fluorescence and reflectance techniques can be used as a comparison to observe physiological and biochemical changes in fruit in pre-harvest and post-harvest (Hoffman *et al*. 2015). Reflectance imaging is a technique in machine vision and image processing that focuses on measuring and analyzing light reflected from the surface of an object. Reflectance in the context of machine vision refers to the ability of a surface to reflect the light it receives (Cubero *et al*. 2011). Fluorescence imaging is a technique used to detect and measure light emitted by an object after being illuminated by light at a certain wavelength. Fluorescence occurs when a molecule (called a fluorophore) absorbs light at a certain wavelength and then emits light at a longer wavelength. Biological materials, after being excited by absorbing ultraviolet (UV) radiation or visible light with a short wavelength, can emit radiation with a longer wavelength (Wang *et al*. 2013; Pan *et al*. 2017). The use of computer vision combined with artificial neural networks has been carried out to predict the phenol content, pH, and authenticity of civet coffee beans (Hendrawan *et al.* 2019). The use of reflectance and fluorescence images to predict the ripeness of citrus fruits using a regression model on a convolutional neural network (Al Riza *et al.* 2024), as well as the use of hyperspectral imaging to detecting chemical, biological, and physical properties of herbal injections (Zhong *et al.* 2022), assessing quality of apple fruits (Cetin *et al.* 2022).

In this study, computer vision combined with Artificial Neural Network (ANN) modeling was used to identify and predict phenol content in red betel leaves. ANN as one of the most effective predictive modeling methods for handling complex and non-linear data such as reflectance and fluorescence image data. ANN is able to learn from complex data patterns to make accurate predictions, making it a powerful tool in modeling the relationship between plant images and bioactive content, including phenol. Prediction of phenol content in red betel leaves can help determine the potential health benefits of leaves in developing more effective herbal products or supplements, may assist in production standards and ensure product consistency, and can help determine the appropriate processing and storage processes to maintain the quality and effectiveness of red betel leaves. Learning function and activation function are one of the factors that can affect the performance of artificial neural networks to find optimal results (Kani and Ghahremani 2024; Mishra *et al.* 2024). Activation functions play a role in extraction and prediction, learning patterns in datasets, helping to automate feature detection, and increasing the learning speed of ANN (Sharma *et al.* 2020). The selected activation function is tansig, a hyperbolic tangent training function that calculates the output layer from the input (Geetha *et al.* 2021). The tansig activation function used in the ANN model has shown results with high accuracy (Lee *et al.* 2020). In the learning process, the method commonly used is backpropagation, a simple algorithm that changes weights based on gradient descent (Jeyasothy *et al.* 2024). This study was aimed to build a prediction model for phenol content in red betel leaves using reflectance and fluorescence image data combined with the ANN method.

Materials and Methods

Experimental details and treatments

Experimental material: The materials used in this study were red betel leaves (*Piper crocatum* Ruiz & Pav.) from Malang, East Java, Indonesia. Red betel leaf samples consisted of three levels of chlorophyll based on SPAD-502 Plus Chlorophyll Meter (Konica Minolta), namely low SPAD (30–45 cci), medium SPAD (46–60 cci), and high SPAD (61–75 cci). The number of leaves was used 25 leaves for each level, so that the total number of image data leaf samples was 75 leaves. Testing of phenol content used gallic acid, 99% ethanol, folin-ciocalteliu reagent (FCR) and sodium carbonate (Na_2CO_3).

Treatments: Red betel leaves were picked from 07.00 to 08.00 AM, avoiding high ambient temperature due to sun and maintaining the content of active substances such as phenol compounds, flavonoids, and essential oils which tend to be higher in the morning. It was ensured that the betel leaves to be used were in healthy condition (no brown spots on the leaves).

Measurement of total phenol

The first stage carried out in the phenol test was the preparation of a standard solution (calibration curve), using gallic acid with a concentration of 20, 40, 60, 80 and 100 ppm. A total of 0.5 mL of FCR reagent and 2.5 mL of Na_2CO_3 were added to each standard solution and shaken slowly with a vortex. Then incubation was carried out for 30 min at room temperature, so that the greenish blue color was fully formed. The absorbance of each standard solution was measured at a wavelength of 746 nm using a UV-Vis spectrophotometer. Then a calibration curve was made between concentration and absorbance to obtain a linear regression equation.

The next stage was the extraction process 1 g of red betel leaves was extracted with 25 mL of 99% ethanol using the maceration method. The phenolic compounds from the mixture were soaked for 30 min, then shaken with a Thermoscientific compact digital orbital shaker at a speed of 150 rpm for 4 h. The betel leaf extract was then filtered. The total amount of phenolic compounds was determined using a UV–Vis spectrophotometer using FCR (Złotek *et al.* 2014). A sample of 0.5 mL of red betel leaf extract was added with 2 mL of 10% FCR and 2.5 mL of 7.5% sodium carbonate. Homogenization was done using a Thermoscientific LP orbital type vortex at a speed of 3000 rpm for 3 sec. The sample solution was incubated at room temperature for 30 min, then its absorbance was measured at 746 nm using a UV–Vis spectrophotometer (Shimadzu UV-1280) (Lee *et al.* 2003). The total phenol content (TPC) in the leaves was calculated using the formula:

$$\text{TPC (mg GAE/g)} = \frac{c \ x \ v}{g}$$

Where: c = phenolic concentration (mg/L)
v = extract volume (mL)
g = weight of sample (g).

Image

Image acquisition was carried out using a 50 x 50 x 60 cm mini studio, equipped with a Canon EOS 700D digital camera, a 50 W white LED halogen lamp, and an LDR2-100UV3-365-N UV lamp. Image acquisition was performed with a distance between the camera and the object of 33.5 cm. Image acquisition using the reflectance method was conducted using light from four white LED lamps to assist lighting when taking images. Camera settings for reflectance image acquisition were manual mode with an ISO 100 configuration, aperture 5.6, and exposure time 1/20 sec. Image acquisition using the fluorescence method was carried out using light from a UV lamp. A UV bandpass filter was placed in front of the UV light source and the camera to block reflected light. Camera settings for fluorescence image acquisition were manual mode with an ISO 100 configuration, aperture 5.6, and exposure time of 2 sec. The captured image had a JPG format measuring 3456 x 5184 pixels with a resolution of 72 dpi. Non-destructive image data capture is illustrated in Fig. 1.

Feature

Image segmentation was a method used in the data preprocessing stage to separate objects in an image from the background of the image (Isa-Jara *et al.* 2022). Image preprocessing involved separating objects from the

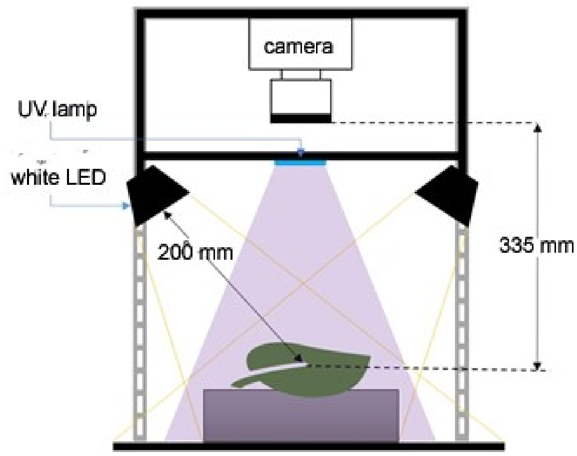

Fig. 1: Image acquisition scheme with reflectance and fluorescence imaging

background in an image and extracting color features in reflectance and fluorescence images. The color feature extraction process was carried out using the Google Colab application with RGB, Lab*, and HSV models, the results of which were numeric data. The color features of the image were used as input data and the total phenol content was used as output data. Before entering the data into the classification and regression models, image processing was carried out to extract color features. Color feature extraction involved calculating the average value of each pixel in the sample. The color features used included RGB, Lab*, and Color feature extraction used Google colab with the Python programming language, and the background and noise were removed using Adobe Photoshop CS6 version 13.0.1.

ANN model

The ANN model was built using a feed-forward structure type and a back-propagation algorithm. This back-propagation feed-forward network consisted of an input layer, hidden layers, and an output layer. The number of hidden layers and the number of nodes in each hidden layer was determined based on the trial-and-error method (Sinshaw *et al.* 2019). The ANN model in this study used 75 data from reflectance images, 75 data from fluorescence images, and 75 data from total phenol content. The color features of the image were used as input data and the total phenol content was used as output data. The collected dataset was divided into two types of data, namely training data and validation data. Training data were used to build and train the ANN model, while validation data were used to validate the ANN model. The images were trained (training data) and validated (validation data) using ANN modeling. 75% of the total data was used as training data and 25% as validation data. Designing the best ANN topology was done through sensitivity analysis to evaluate how the parameters in the output layer respond to variations given to the components of the ANN model builder, such as the learning function, activation function, learning rate, and momentum (0.1, 0.5, 0.9), the number of hidden layers (1 or 2) and the number of nodes (10, 20, 30, 40). There was selection of learning functions including Traincgb, Traincgf, Traincgp, Traingd, Traingdm, Traingda, Traigdx, Trainlm, Trainoss, Trainrp, and Trainscg, while the activation function consisted of tansig, logsig, and purelin. Matlab R2021a version 9.10.0.1602886 was used to build the ANN model to find the best modeling topology. The ANN model evaluation used two main parameters, namely mean squared error (MSE) and R-squared (R^2). The best ANN model was selected based on the lowest validation MSE value and the highest R^2 value. A low MSE indicates a small prediction error, while a high R^2 indicates the model's ability to explain data variability well. This evaluation process involved comparing the MSE and R^2 values of each model on the validation dataset, as well as a comparative analysis of the results of the ANN model trained using reflectance and fluorescence image data. This analysis was aimed at evaluating differences in model performance based on the type of image used.

Results

Image

Image analysis was conducted to determine the differences in reflectance and fluorescence images of leaves with varying phenol content. The image of red betel leaf from reflectance and fluorescence was presented in Fig. 2. This image shows how the reflectance and fluorescence images of red betel leaves changed along with the variation of chlorophyll content (SPAD). The results of the reflectance image tended to have green leaves with red spots while the fluorescence image had red mixed with blue. The reflectance image of leaves with high SPAD had greener than the leaves with medium or low SPAD. The image of the red betel leaf with low SPAD reflectance had a pale green color indicating low chlorophyll content. Phenol analysis on red betel leaves showed that red betel leaves with a range of 30–45 cci had an average phenol value of 5993.2 mg GAE/g, in the range of 46–60 cci had an average phenol value of 4960.8 mg GAE/g, while in the range of 61–75 cci had an average phenol value of 4632.1 mg GAE/g. Leaves with a low SPAD range with a high phenol value absorbed UV waves so that chlorophyll did not emit red.

ANN

Several factors affected the ANN modelling results, which include architecture, activation function, and learning function used. Determination of the ANN architecture was done by combining hyperparameters in the form of learning rate, momentum, number of hidden layers and number of neurons in the hidden layer. Learning rate determined how

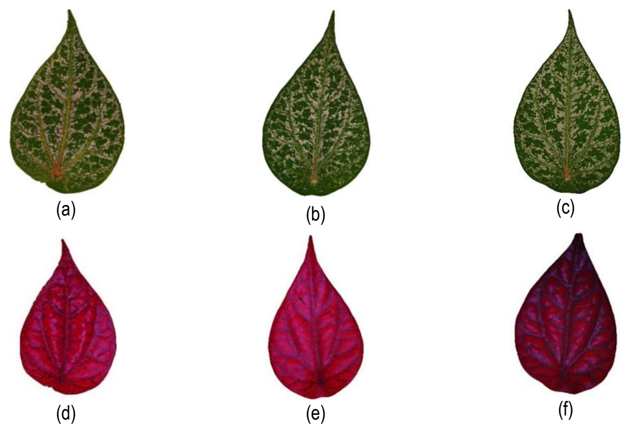

Fig. 2: Red betel leaf image results of reflectance and fluorescence; (a) low SPAD reflectance, (b) medium SPAD reflectance, (c) high SPAD reflectance, (d) low SPAD fluorescence, (e) medium SPAD fluorescence; (f) high SPAD fluorescence

fast the ANN model updates the weights during the training process, with the values tested being 0.1, 0.5 and 0.9. Momentum was used to accelerate the convergence process in ANN training and avoid traps in local minima, with the values tested being 0.1 and 0.5. The number of hidden layers used to construct the ANN structure consisted of 2 hidden layers. The selection of the ANN architecture is done by trial and error, the results of the trial and error selection of the ANN architecture on reflectance and fluorescence data are shown in Table 1.

The performance parameters of the ANN feature selection model were based on the lowest validation MSE parameter, indicating how much error there was between the predicted value and the actual value. The smaller the MSE value, the better the model performance. An R^2 value closer to 1 indicates that the model has good predictive ability, both on training data and testing data (validation). In reflectance data, the lowest validation MSE value (0.08803) with the highest validation R^2 value (0.79444) had a learning rate of 0.1, momentum of 0.9, and an ANN structure with 2 hidden layer structure consisting of 20 nodes and 30 nodes. Meanwhile, the lowest validation MSE value (0.57078) and the highest validation R^2 value (0.43668) on the fluorescence data had a learning rate value of 0.1, momentum of 0.9, and an ANN structure with 2 hidden layers consisting of 20 nodes and 10 nodes. Reflectance data with ANN structure 20-30-1, learning rate 0.9, and momentum 0.5 gave the best results in predicting phenol in red betel leaves compared to fluorescence data.

This learning process was important for training the ANN model in processing data. During the learning process, synaptic connections were adjusted by repeatedly changing weights to minimize errors. Then the activation function played an important role in achieving optimal performance for artificial neural networks. The activation function was

Table 1: Trial and error results of selecting architecture for reflectance and fluorescence data

Data set	Learning Rate	Momentum	ANN structure	R^2 training	R^2 validation	MSE training	MSE validation
Reflectance	0,1	0,1	10-20-1	0.97984	0.66471	0.00854	0.15145
		0,5	30-10-1	0.97836	0.64322	0.00885	0.16963
		0,9	**20-30-1**	**0.97771**	**0.79444**	**0.00903**	**0.08803**
	0,5	0,1	40-10-1	0.98067	0.67824	0.00801	0.11704
		0,5	20-10-1	0.99212	0.56048	0.00422	0.18239
		0,9	10-20-1	0.97821	0.65137	0.00893	0.17117
	0,9	0,1	20-10-1	0.97726	0.69427	0.00919	0.11420
		0,5	30-40-1	0.98981	0.69102	0.00479	0.15655
		0,9	10-30-1	0.98509	0.73357	0.00730	0.11279
Fluorescence	0,1	0,1	10-20-1	0.98003	0.42353	0.00971	0.33055
		0,5	40-20-1	0.98060	0.30408	0.00955	0.62608
		0,9	**20-10-1**	**0.98322**	**0.43668**	**0.00813**	**0.57078**
	0,5	0,1	10-40-1	0.98087	0.29525	0.00927	5.49891
		0,5	40-20-1	0.98039	0.27142	0.00993	1.46497
		0,9	10-20-1	0.99318	0.27106	0.00340	0.43040
	0,9	0,1	20-30-1	0.98446	0.32079	0.00772	0.43243
		0,5	10-40-1	0.98409	0.27280	0.00787	0.90172
		0,9	10-30-1	0.99377	0.23052	0.00340	0.32542

Table 2: Trial and error results for selecting learning functions and activation functions for reflectance and fluorescence data

Data set	Learning function	Activation function			R^2		MSE	
		Hidden Layer 1	*Hidden Layer* 2	Output Layer	Training	Validation	Training	Validation
Reflectance	**Trainlm**	**Tansig**	**Tansig**	**Purelin**	**0.97771**	**0.79444**	**0.00903**	**0.08803**
	Traincgb	Tansig	Tansig	Tansig	0.97560	0.69961	0.00984	0.11613
	Traincgf	Logsig	Logsig	Tansig	0.97525	0.74149	0.00999	0.11545
	Traincgp	Logsig	Logsig	Purelin	0.97766	0.65716	0.00946	0.12611
	Traingd	Tansig	Tansig	Tansig	0.97803	0.60711	0.01000	0.16270
	Traingda	Logsig	Logsig	Tansig	0.97577	0.62470	0.01000	0.14645
	Traingdm	Logsig	Logsig	Logsig	0.55822	0.71131	0.40175	0.40507
	Traingdx	Logsig	Logsig	Logsig	0.34040	0.72782	0.40172	0.40508
	Trainoss	Logsig	Logsig	Tansig	0.97570	0.75801	0.00992	0.09690
	Trainrp	Tansig	Tansig	Tansig	0.97586	0.65276	0.00989	0.12832
	Trainscg	Tansig	Tansig	Tansig	0.97579	0.59763	0.00988	0.15226
Fluorescence	Trainlm	Tansig	Tansig	Purelin	0.98322	0.43668	0.00813	0.57078
	Traingp	Tansig	Tansig	Logsig	0.40365	0.33801	0.08288	0.18870
	Traincgf	Logsig	Logsig	Purelin	0.97969	0.30496	0.00980	0.37785
	Traincgp	Logsig	Logsig	Tansig	0.97973	0.31798	0.00988	0.32306
	Traingd	Tansig	Tansig	Tansig	0.97993	0.37909	0.01000	0.25505
	Traigda	Logsig	Logsig	Purelin	0.91992	0.29573	0.03771	0.32193
	Traingdm	Logsig	Logsig	Purelin	0.80267	0.20255	0.08730	0.54172
	Traingdx	Logsig	Logsig	Purelin	0.97817	0.16892	0.01083	0.56645
	Trainoss	Logsig	Logsig	Purelin	0.97924	0.35975	0.00998	0.33427
	Trainrp	**Tansig**	**Tansig**	**Purelin**	**0.97962**	**0.44367**	**0.00998**	**0.43680**
	Trainscg	Logsig	Logsig	Tansig	0.21909	0.20820	0.40366	0.33801

responsible for processing input data into output data. The results of the trial and error selection of learning functions and activation functions for reflectance and fluorescence data are shown in Table 2.

Table 2 helped determine the optimal configuration for learning and activation functions in the ANN model based on the type of data used (reflectance or fluorescence). The best activation functions obtained were tansig on the hidden layer and purelin on the output layer for both reflectance and fluorescence results. with validation MSE values of 0.08803 (reflectance) and 0.43680 (fluorescence), respectively. In this study, Trainlm and Trainrp were the most optimal learning algorithms.

Pureline is a linear function whose input and output values. In reflectance data, the combination of Trainl (learning function), Tansig (activation function on hidden layers 1 and 2), and Purelin (activation function on output layer) gave the best results. This is indicated by the highest R^2 validation value of 0.79444 and the lowest MSE validation of 0.08803. This combination succeeded in providing more accurate prediction results compared to other functions on reflectance data. For fluorescence data, the combination of Trainrp (learning function), Tansig (activation function on hidden layers 1 and 2), and purelin (activation function on output layer) gave the best performance with R^2 validation of 0.44367 and MSE validation of 0.43680. This showed that the overall fluorescence prediction performance was lower than reflectance, but this combination gave the best results for fluorescence data. The architecture of the image processing results with RGB, HSV, Lab* input layers for reflectance and fluorescence data is shown in Fig. 3.

Analysis of the best modelling of reflectance and fluorescence images

After obtaining the model from the ANN reflectance data and the ANN model of fluorescence data, a correlation coefficient graph was also obtained from the training and validation results and a graph of the relationship between iteration and MSE. Results of the training of reflectance data and fluorescence data are presented in Fig. 4. During training, fluorescence had a greater R value compared to the R value of reflectance data. The R value during training was a correlation coefficient that describes the strength of the relationship between the independent variable and the dependent variable during the data training process.

Fig. 5 shows that when validating the reflectance data, the R value was greater than the R value of the fluorescence data. The results of the validation of the reflectance data had a strong value of 0.8, while for the fluorescence data it was still classified as moderate, at 0.4.

Fig. 6 shows that as the iteration increased, the MSE value decreased, which was due to the network's stable ability to recognize patterns. A decrease in the relationship between iteration and MSE indicated that the training data were achieved well. The maximum number of epochs was determined, namely 10,000 with a goal of 0.01. This treatment means that the training data would stop when the epoch reached 10,000 or when the goal of 0.01 was achieved. The determination of the maximum epoch and goal aimed to avoid overfitting in the model.

Discussion

This study introduced a novel approach to predicting phenol content in red betel leaves by directly comparing the efficacy of reflectance and fluorescence imaging techniques when combined with artificial neural network (ANN) modeling. The key finding was that the reflectance-based ANN model significantly outperformed the fluorescence-based model in predicting phenol content, as evidenced by a lower validation MSE of 0.08803 and a higher validation R^2 of 0.79444. In contrast, the fluorescence-based model yielded a higher validation MSE of 0.43680 and a lower R^2 of 0.44367. The MSE value was an important performance factor indicating the accuracy of the ANN model; the lower the MSE value, the higher the accuracy. The R value ranged from 0 to 1, where values closer to 1 indicated a smaller difference between the predicted and actual data. An R^2 value greater than 0.8 was considered satisfactory (Chen *et al.* 2022). In this study, the R^2 value for fluorescence images remained below 0.8, but determining the best ANN modeling for phenol content prediction also involved considering the lowest MSE value and the highest R^2. The correlation coefficient value had been divided into several criteria, namely 0.00–0.19 as very low, 0.20–0.39 as low, 0.40–0.59 as moderate, 0.60–0.79 as strong, and 0.80–1.00 as very strong (Ryan and Bruno 2017).

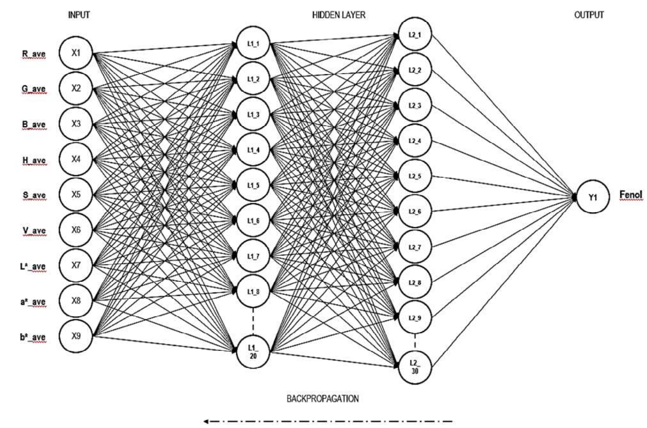

(a) ANN model of reflectance

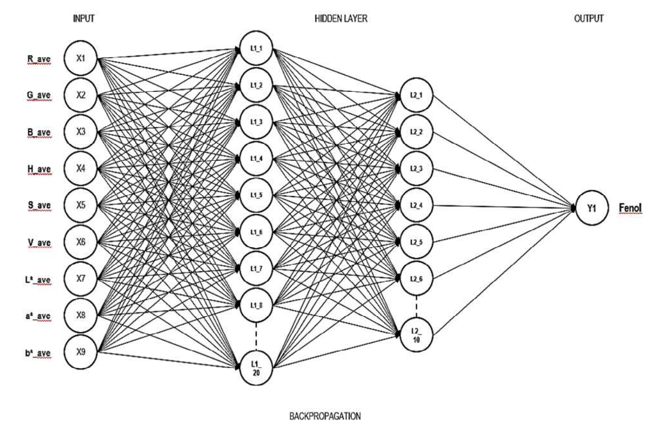

(b) ANN model of fluorescence

Fig. 3: ANN modeling architecture

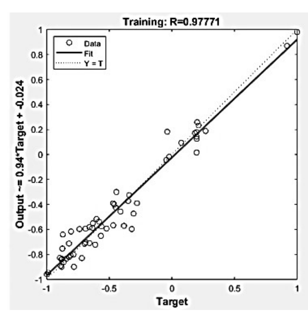

(a)

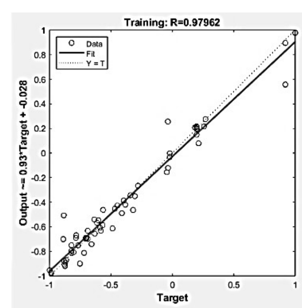

(b)

Fig. 4: Training results: (a) reflectance data, (b) fluorescence data

The reflectance images revealed that leaves with higher chlorophyll content (high SPAD values) exhibited a darker green color, whereas those with lower chlorophyll content (low SPAD values) appeared pale green. This correlation aligns with previous studies indicating that chlorophyll concentration influences leaf coloration (Wu *et al.* 2024). In fluorescence images, leaves with low SPAD values showed

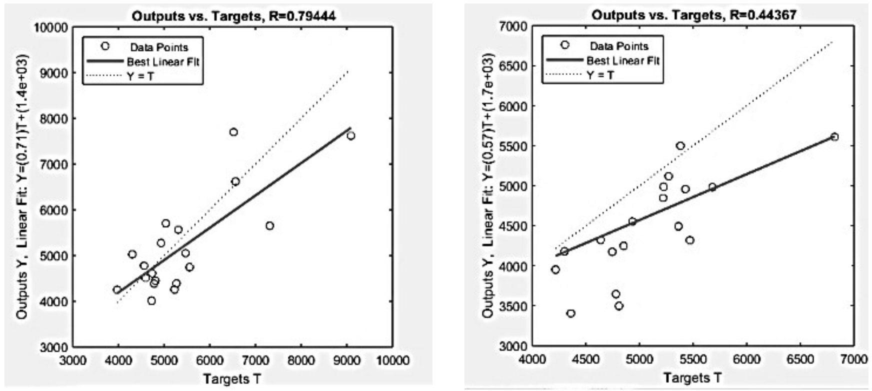

(a) (b)

Fig. 5: Validation results (a) reflectance data, (b) fluorescence data

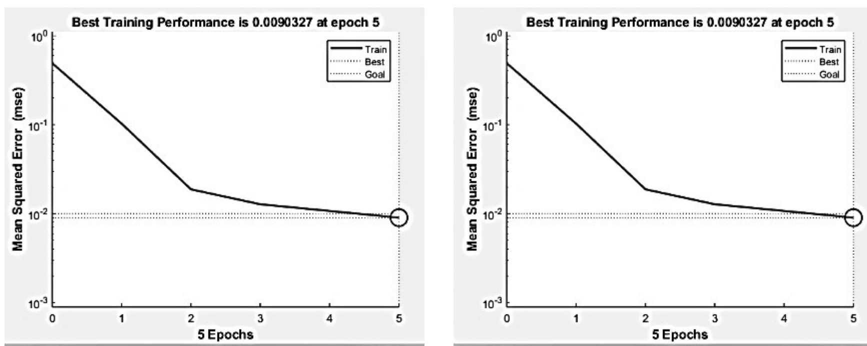

(a) (b)

Fig. 6: Relationship MSE and iteration; (a) reflectance data, (b) fluorescence data

bright red fluorescence, suggesting a strong fluorescence signal due to lower chlorophyll absorption of ultraviolet (UV) light. As SPAD values increased, the fluorescence intensity decreased, resulting in darker images. This inverse relationship was consistent with the understanding that chlorophyll molecules absorbed more UV light, reducing fluorescence emission at higher chlorophyll concentrations (Meyer *et al*. 2003). Interestingly, the presence of blue hues in some fluorescence images was attributed to the emission from the leaf's cell walls, which fluoresce blue under UV illumination (Kumachova *et al.* 2022). Phenolic compounds, such as flavonoids located in the epidermis, absorbed UV light and could quench chlorophyll fluorescence (Abdallah *et al.* 2018). Leaves with higher phenol content (low SPAD values) thus displayed stronger fluorescence due to reduced chlorophyll absorption.

The superior predictive performance of the reflectance-based ANN model may have been attributed to the direct interaction between incident light and phenolic compounds on the leaf surface. Reflectance imaging captured variations in leaf color and texture influenced by phenolic content, which affected the absorption and reflection of specific wavelengths in the visible spectrum. Phenolic compounds often had characteristic absorption features that can be effectively detected through reflectance measurements, enhancing the ANN's ability to learn and predict phenol levels accurately. In contrast, fluorescence imaging depended on the emission of light from excited molecules, which could be influenced by environmental conditions, the presence of other fluorophores, and quenching effects. This complexity introduced additional variability and noise into the fluorescence data, reducing the ANN's predictive accuracy.

The study also highlights the importance of optimizing ANN parameters to achieve optimal predictive performance. For the reflectance data, the combination of the Levenberg-Marquardt algorithm (Trainlm) as the learning function, the hyperbolic tangent sigmoid (tansig) activation function in the hidden layers, and a linear (purelin) activation function in the output layer resulted in the best performance (Fan *et al*. 2022; Jee *et al.* 2023). This configuration effectively modeled the non-linear relationships between the input color features and phenol content, facilitating efficient learning and accurate predictions. For the fluorescence data, although the same activation functions were used, the resilient backpropagation algorithm (Trainrp) served as the learning function. However, the fluorescence-based model still underperformed compared to the reflectance-based model, suggesting that the type of imaging data plays a more critical role than the choice of learning algorithms and activation functions.

This study was among the first to directly compare reflectance and fluorescence imaging techniques for predicting phenol content in plant leaves using ANN modeling. The novelty of this comparative analysis lay in demonstrating that reflectance imaging provided superior predictive performance for phenol content compared to fluorescence imaging, thereby offering new insights into the effectiveness of non-destructive optical methods. Previous studies utilized imaging methods separately for various applications, such as assessing fruit ripeness or detecting other bioactive compounds (Hendrawan *et al*. 2019; Al Riza *et al*. 2024). By showing that reflectance imaging led to more accurate and robust phenol predictions than fluorescence imaging, this study provided valuable guidance for future research and practical applications in non-destructive plant analysis. These findings had significant implications for agriculture and the herbal product industry. Utilizing reflectance imaging combined with ANN modeling offered a rapid, non-destructive, and cost-effective method for estimating phenol content in red betel leaves. This approach could facilitate real-time monitoring of plant quality, enabling producers to optimize harvest timing and ensure consistent phenolic content in herbal products. It reduced reliance on time-consuming and destructive chemical analyses, streamlining quality control processes and potentially improving product standardization.

One limitation of the study was the relatively low validation R^2 value for the fluorescence-based model, possibly due to environmental and biological factors such as inconsistent lighting conditions and natural variability in wild-collected samples. Future studies should consider controlling environmental variables during data collection and increasing sample size to enhance model robustness. Additionally, exploring other machine learning algorithms or integrating spectral data from hyperspectral imaging could further improve predictive accuracy. Despite this limitation, the novelty and findings of this work provided a strong foundation for future advancements in non-destructive phenol content estimation in red betel leaves and other plant materials.

Conclusion

The best ANN modeling obtained from reflectance image data produced a validation MSE of 0.08803 and a validation R value of 0.79444, while the best ANN modeling from fluorescence image data resulted in a validation MSE of 0.43680 and a validation R value of 0.44367. These findings indicated that ANN modeling on reflectance images showed superior performance for predicting phenol content in red betel leaves. The resulting ANN modeling architecture included RGB, HSV, Lab* input layers, two hidden layers consisting of 20 nodes and 30 nodes, a learning rate of 0.1, and a momentum of 0.9. The use of the hyperbolic tangent sigmoid (tansig) activation function in the hidden layers and a linear (purelin) activation function in the output layer, along with the Levenberg-Marquardt (Trainlm) learning algorithm, significantly enhanced the model's predictive accuracy. This novel reflectance-based approach provided a more accurate and efficient predictive model, thereby potentially serving as a basis for the development of real-time plant quality monitoring technology in the future.

Acknowledgements

The authors wish to thank Rut Juniar Nainggolan and Mitha Sa'diyah for their work in assisting with sample data collection.

Author Contributions

RD conducted research and wrote manuscript; YH reviewed data processing and reviewed the manuscripts; S conducted research and reviewed manuscript; BDA reviewed the manuscript.

Conflicts of Interest

The authors assert that they have no conflicts of interest to declare.

Data Availability

The data can be obtained from the corresponding author upon a reasonable request.

Ethics Approval

Not applicable.

References

Abdallah FB, W Philippe, JP Goffart (2018). Comparison of optical indicators for potato crop nitrogen status assessment including novel approaches based on leaf fluorescence and flavonoid content. *J Plant Nutr* 41: 2705–2728

Al Riza DF, AM. Ikrom, AA Tulsi, Darmanto, Y Hendrawan (2024). Mandarin orange (Citrus reticulata Blanco cv. Batu 55) ripeness parameters prediction using combined reflectance-fluorescence images and deep convolutional neural network (DCNN) regression model. *Sci Hortic* 331:113089

Cetin N, K Karaman, E Kavuncuoğlu, B Yıldırım, A Jahanbakhshi (2022). Using hyperspectral imaging technology and machine learning algorithms for assessing internal quality parameters of apple fruits. *Chemometrics Intelligent Laboratory Syst* 230:104650

Chan FWY (2010). Measurement sensivity enhancement by improved reflective computer vision technique for non-destructive evaluation. *NDTE Intl* 43:210–215

Chen WY, YJ Chan, JW Lim, CS Liew, MHCD Mohamad, A Usman, G Lisak, H Hara, WN Tan (2022). Artificial neural network (ANN) modelling for biogas production in pre-commercialized integrated anaerobic-aerobic bioreactors (IAAB). *Water* 14:1410

Cubero S, N Aleixos, E Molto, J Gomez-Sanchis, J Blasco (2011). Advances in machine vision applications for automatic insepction and quality evaluation of fruits and vegetables. *Food Bioproc Technol* 4:487–507

Edo GI, SC Nwachukwu, ABM Ali, E Yousif, AN Jikah, K Zainulabdeen, HA Ekokotu, EF Isoje, UA Igbuku, RA Opiti, PO Akpoghelie, JO Owheruo, AEA Essaghah (2024). A review on the composition, extraction and applications of phenolic compounds. *Ecol Front* 00:00000 https://doi.org/10.1016/j.ecofro.2024.09.008

Fan G, AS El-Shafay, SA Eftekhari, M Hekmatifar, D Toghraie, AS Mohammed, A Khan (2022). A well-trained artificial neural network (ANN) using the trainlm algorithm for predicting the rheological behavior of water – Ethylene glycol/WO3 – MWCNTs nanofluid. *Intl Commun Heat Mass Transfer* 131:105857

Geetha K, SV Reddy, B Sarojamma (2021). Effects and analysis of activation functions in artificial neural networks using NN tool in matlab on weather parameters. *J Emerg Technol Innov Res* 8:a609–a612

Hendrawan Y, S Widyaningtyas, S Sucipto (2019). Computer vision for purity, phenol, and pH detection of Luwak coffee green bean. *Telkomnika* 17:3073–3085

Hoffmann AM, G Noga, M Hunsche (2015). Fluorescence indices for monitoring the ripening of tomatoes in pre- and postharvest phases. *Sci Hortic* 191:74–81

Isa-Jara R, C Pérez-Sosa, E Macote-Yparraguirre, N Revollo, B Lerner, S Miriuka, C Delrieux, M. Pérez, R. Mertelsmann (2022). GEMA—An automatic segmentation method for real-time analysis of mammalian cell growth in microfluidic devices. *J Imaging* 8:281

Jee HJ, SH Yeon, J Park, Y Yoon, KH Lee (2023). Machine learning based simultaneous control of air handling unit discharge air and condenser water temperatures set-point for minimized cooling energy in an office building. *Ener Build* 297:113471

Jeyasothy A, S Ramasamy, S Sundaram (2024). A gradient descent algorithm for SNN with time-varying weights for reliable multiclass interpretation. *Appl Soft Comput* 161:111747

Kani GT, A Ghahremani (2024). Optimal design of heat pipes for city gate station heaters by applying genetic and Bayesian optimization algorithms to an artificial neural network model. *Case Stud Therm Eng* 55:104203

Kaushal S, DK Tammineni, P Rana, M Sharma, K Sridhar, H Chen (2024). Computer vision and deep learning-based approaches for detection of food nutrients/nutrition: New sights and advances. *Trends Food Sci Technol* 146:104408

Kumachova T, B Alexander, R Andrey (2022). Outer and internal cuticle in the leaves of *Malus* (Rosaceae) in mountains and plains. *Microsc Res Tech* 85:3439–3454

Lee DH, YT Kim, SR Lee (2020). Shallow landslide susceptibility models based on artificial neural networks considering the factor selection method and various non-linear activation functions. *Remote Sens* 12:1194

Lee KW, YJ Kim, HJ Lee, CY Lee (2003). Cocoa has more phenolic phytochemical and higher antioxidant than teas and red wine. *J Agric Food Chem* 51:249–252

Li S, H Luo, M Hu, M Zhang, J Feng, Y Liu, Q Dong, B Liu (2019). Opctical non-destructive techniques for small berry fruits: A review. *Artif Intellig Agric* 2:85–98

Li Z, D Wang, T Zhu, Y Tao, C Ni (2024). Review of deep learning-based methods for non-destructive evaluation of agricultural products. *Biosyst Eng* 245:56–83

Lu Y, W Saeys, M Kim, Y Peng, R Lu (2020). Hyperspectral imaging technology for quality and safety evaluation of horticultural products: A review and celebration of the past 20-year progress. *Postharv Biol Technol* 170:111318

Meyer S, A Cartelat, I. Moya, Z G Cerovic (2003). UV-induced blue-green and far-red fluorescence along wheat leaves: A potential signature of leaf ageing. *J Exp Bot* 54:757–769

Mishra SR, PK Pattnaik, R Baithalu, PK Ratha, S Panda (2024). Predicting heat transfer Performance in transient flow of CNT nanomaterials with thermal radiation past a heated spinning sphere using an artificial neural network: A machine learning approach. *Partial Differ Eq Appl Maths* 12:100936

Pan L, Y Sun, H Xiao, X Gu, P Hu, Y Wei, K Tu (2017). Hyperspectral imaging with different illumination patterns for the hollowness classification of white radish. *Postharv Biol Technol* 126:40–49

Ryan N, P Bruno (2017). Analysis of 3D multi-segment lumbar spine motion during gait and prone hip extension. *J Electromyogr Kinesiol* 33:111–117

Sharma S, S Sharma, A Athaiya (2020). Activation functions in neural networks. *Intl J Eng Appl Sci Technol* 4:310–316

Singh T, P Singh, VK Pandey, R Singh, AH Dar (2023). A literature review on bioactive properties of betel leaf (*Piper betel* L.) andits applications in food industry. *Food Chem Adv* 3:100536

Sinshaw TA, CQ Surbeck, H Yasarer, Y Najjar (2019). Artificial neural network for prediction of total nitrogen and phosphorus in US lakes. *J Environ Eng* 145:04019032

Tran VT, TB Nguyen, HC Nguyen, NHN Do, PK Le (2023). Recent application of natural bioactive compounds from *Piper betle* (L.) leaves in food preservation. *Food Cont* 154:110026

Wang H, C Li, M Wang (2013). Quantitative determination of onion internal quality using reflectance, interactance and transmittance modes of hyperspectral imaging. *Trans ASABE*, 56:1623–1635

Wu L, Y Zhang, Z Zhang, X Zhang, Y Wu, JM Chen (2024). Deriving photosystem-level red chlorophyll fluorescence emission by combining leaf chlorophyll content and canopy far-red solar-induced fluorescence: Possibilities and challenges. *Remote Sens Environ* 304:114043

Zhong Y, C Ru, S Wang, Z Li, Y Cheng (2022). An online, non-destructive method for simultaneously detecting chemical, biological, and physical properties of herbal injections using hyperspectral imaging with artificial intelligence. *Spectrochim Acta Part A: Mol Biomol Spectrosc* 264:120250

Złotek U, M Świeca, A Jakubczyk (2014). Effect of abiotic elicitation on main health-promoting compounds, antioxidant activity and commercial quality of butter lettuce (*Lactuca sativa* L.). *Food Chem* 148:253–260